SCIENTIFIC REPORTS

OPEN

SUBJECT AREAS:
MECHANICAL PROPERTIES
ELECTRONIC DEVICES
ELECTRICAL AND ELECTRONIC ENGINEERING
METALS AND ALLOYS

Received
20 September 2012

Accepted
1 March 2013

Published
15 March 2013

Correspondence and requests for materials should be addressed to Y.Z. (drzhangy@ustb.edu.cn) or P.K.L. (pliaw@utk.edu)

# High-entropy Alloys with High Saturation Magnetization, Electrical Resistivity, and Malleability

Yong Zhang[1], TingTing Zuo[1], YongQiang Cheng[2] & Peter K. Liaw[3]

[1]State Key Laboratory for Advanced Metals and Materials, University of Science and Technology Beijing, Beijing 100083, China, [2]Chemical and Engineering Materials Division, Oak Ridge National Laboratory, Oak Ridge, TN 37831, USA, [3]Department of Materials Science and Engineering, The University of Tennessee, Knoxville, TN 37996, USA.

**Soft magnetic materials (SMMs) find important applications in a number of areas. The diverse requirements for these applications are often demanding and challenging for the design and fabrication of SMMs. Here we report a new class of FeCoNi(AlSi)$_x$ ($0 \le x \le 0.8$ in molar ratio) SMMs based on high-entropy alloys (HEAs). It is found that with the compositional and structural changes, the optimal balance of magnetic, electrical, and mechanical properties is achieved at $x = 0.2$, for which the combination of saturation magnetization (1.15 T), coercivity (1,400 A/m), electrical resistivity (69.5 μΩ·cm), yield strength (342 MPa), and strain without fracture (50%) makes the alloy an excellent SMM. Ab initio calculations are used to explain the high magnetic saturation of the present HEAs and the effects of compositional structures on magnetic characteristics. The HEA-based SMMs point to new directions in both the application of HEAs and the search for novel SMMs.**

The newly-developed high-entropy alloys (HEAs) are receiving much attention for their unique structures and excellent properties[1–10]. Unlike traditional alloys, which are normally based on one or two principal elements, HEAs defined by Yeh et al. can have five or more principal elements in equal or near-equal molar ratios[1]. In recent studies, quaternary and ternary alloys in an equal molar ratio are also considered as HEAs[2,3]. The presence of multiple principal elements in HEAs is not merely a difference in composition, but has fundamental physical effects on the configurational entropy, free energy, phase selection, and stability[4]. In general, the high-entropy effect in these alloys can greatly reduce the free energy of simple solid-solution phases, especially at high temperatures, making the chemically-ordered intermetallic compounds less competitive. As a result, HEAs obtained after rapid quenching are often found to contain topologically-simple [e.g., face-centered cubic (FCC) or body-centered cubic (BCC)] yet chemically-disordered solid solutions, nano-sized precipitates, and amorphous phases[1,4,11,12].

The complicated structure at macroscopical and atomic levels may lead to a wide range of properties, some of which are not available in other materials and may be appealing for certain applications. For example, many HEAs exhibit high thermal stability and hardness, great fatigue resistance, as well as excellent corrosion and wear resistance[7,13–15]. These mechanical and electrochemical properties make HEAs promising candidates as refractory materials, diffusion-barrier layers, fatigue-resistant materials, corrosion-resistant surface layers, and wear-resistant materials[7,12–17]. Recently, there has been expectation that some HEAs may also possess excellent magnetic properties[18]. Indeed, there are several reasons to believe that HEAs could make good SMMs, for which high saturation magnetization (to enhance the capacity), electrical resistivity (to suppress the eddy-current loss), and malleability (to facilitate processing and reduce energy cost) are desired, in addition to the low coercivity (i.e., soft magnetism)[19]. First, several ferromagnetic elements with high magnetic moments are known to form HEAs. Second, electrical resistivity may increase due to topological distortion and chemical randomness. Third, the simple crystalline structure (e.g., FCC) provides geometric basis for reasonable malleability. There is a pressing need for such SMMs because very few existing SMMs, if any, can meet all of the above requirements[20–23], e.g., the high silicon steels are brittle at room temperature, the Fe-Ni alloys have low electrical resistivity, and the metallic glasses[24] are relatively unstable, and their sizes are limited by the glass-forming ability. In the present work, we show how a group of new HEAs, FeCoNi(AlSi)$_x$ ($0 \le x \le 0.8$ in a molar ratio), are designed and optimized to achieve an excellent combination of mechanical, electrical, and magnetic properties. The revealed composition

dependence of the structures, properties, and their correlations will shed light on the future development of the high-entropy SMMs.

## Results

We start testing from the ternary FeCoNi alloy (denoted A0) mixing in an equal molar ratio. The resulting saturation magnetization ($M_s$ = 1.315 T) is impressive, and the coercivity ($H_c$ = 1,069 A/m) indicates soft magnetism. However, the electrical resistivity ($\rho$ = 16.7 $\mu\Omega\cdot$cm) is too low (only slightly higher than the pure iron). Then, Al and Si are added, which are expected to increase the electrical resistivity but at the same time sacrifice the magnetization. Figure 1 shows the composition dependence of the saturation magnetization and coercivity in $FeCoNi(AlSi)_x$ ($0 \le x \le 0.8$, the alloy with $x = 0.1$ will be denoted A1, and so on). Indeed, $M_s$ drops almost monotonically upon the additions of Al and Si, from 1.315 T at $x = 0$ (A0) all the way to 0.46 T at $x = 0.8$ (A8). In contrast, the composition dependence of $H_c$ appears rather irregular and unpredictable: $H_c$ is low at $x \le 0.2$, but increases dramatically at $x = 0.3$. It falls back to a low value at $x = 0.5$, before hiking again at $x = 0.8$. The original hysteresis loops and a table listing all the data are included in the supplementary information (Figure S1 and Table S1). Obviously, only $FeCoNi(AlSi)_x$ with $x \le 0.2$ can be considered as SMMs, and the very different composition dependence of $M_s$ and $H_c$ (Figure 1) in fact has its root in the atomic-level and micro-scale structures, as will be discussed later.

Figure 2 presents the electrical resistivity ($\rho$) as a function of Al and Si additions. The general trend is that the electrical resistivity increases from $x = 0$ to $x = 0.8$, with some deviation in the range of $0.3 \le x \le 0.5$. The deviation of $\rho$ from the general trend corroborates the unusual behavior of $H_c$ in the same composition range, as illustrated in Figure 1, suggesting possible common origins (will be discussed later). High electrical resistivity is an important requirement for SMMs used in the high-frequency magnetic field, as it reduces the eddy-current loss[25]. The typical electrical resistivity of the silicon steel is 50 – 80 $\mu\Omega\cdot$cm[26]. Thus, $x > 0.1$ is needed for $FeCoNi(AlSi)_x$ to have similar values.

An important aspect in materials selection is mechanical properties. Although they may not be why the material works, they often profoundly influence how the material is fabricated and how it performs. For example, many SMMs are used in the form of thin plates with a thickness of less than 1 mm, and direct casting for such thickness is usually difficult. The preferred procedure is, therefore, to use cold rolling and annealing to process the bulk materials, in which the malleability of the material is a crucial factor - the higher the malleability, the lower the cost of time and energy to achieve the desired thickness. In Figure 3, we compare the room-temperature compressive engineering stress-strain curves of the as-cast alloys. The extracted data for yield strength, ultimate tensile strength, and plastic strain limits can be found in Table S2. As indicated by the stress-strain curves, when x varies in the range of 0 to 0.2, the alloys exhibit good plasticity and significant work hardening. The plastic deformation ($\varepsilon_p$) exceeds 50% without fracture. The yield strength increases from 208 MPa at $x = 0$ to 342 MPa at $x = 0.2$. The A3 alloy exhibits a much higher yield strength (938 MPa) and the ultimate tensile strength (2,857 MPa), together with good plasticity of 33%. When x is further increased to $\ge 0.4$, the ductility of the alloys diminishes, and the samples become brittle. The extreme case is the A8 alloy, which shatters immediately after elastic deformation, and its ultimate tensile strength is only 1,017 MPa. The A4 and A5 alloys exhibit little plastic deformation too, with plastic strain limits of 2.76% and 0.04%, respectively. However, their yield strength and maximum strength remain high. The composition dependence of the yield strength is also depicted in Figure S2, together with the measured Vickers hardness.

For an in-depth study of these alloys, the information on the atomic-level structure, such as the lattice types and how different species are arranged, are obtained. Figure 4 shows the X-ray diffraction patterns of the $FeCoNi(AlSi)_x$ alloys. The Bragg peaks indicate a single-phase FCC solid solution for $x \le 0.2$. As x approaches 0.3, signature peaks of a BCC structure can be clearly seen, suggesting a BCC + FCC mixture (Figure 4). When x reaches 0.4, the structure turns almost entirely into BCC. Such a transition from the FCC to BCC solid solutions is not uncommon for HEAs, and it in fact has

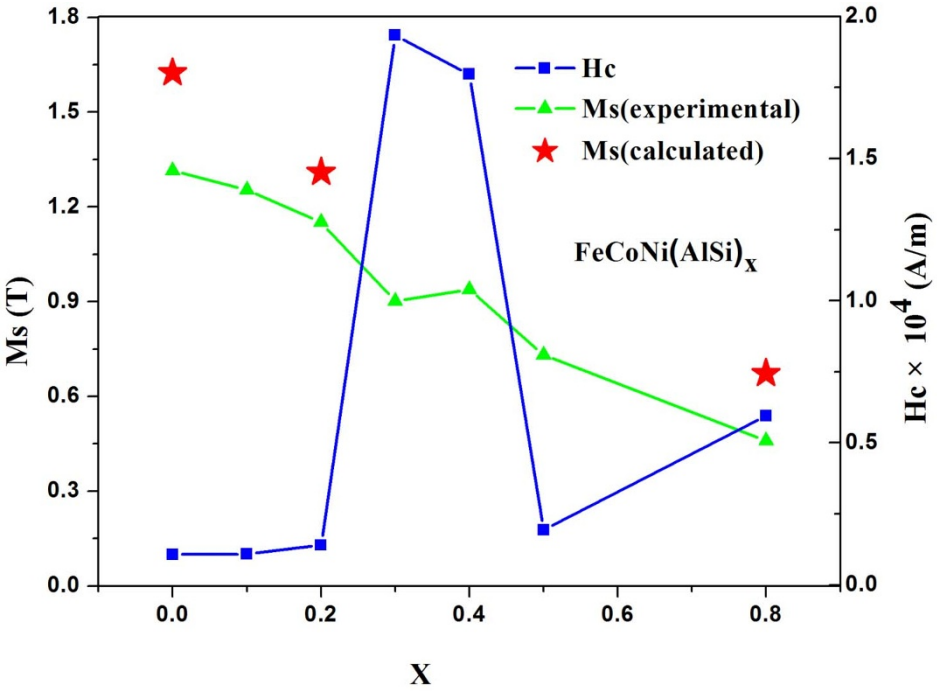


**Figure 1 | Magnetic properties of $FeCoNi(AlSi)_x$ ($x = 0$, 0.1, 0.2, 0.3, 0.4, 0.5, and 0.8) alloys ($H_c$ and $M_s$ represent the coercivity and saturation magnetization, respectively).**

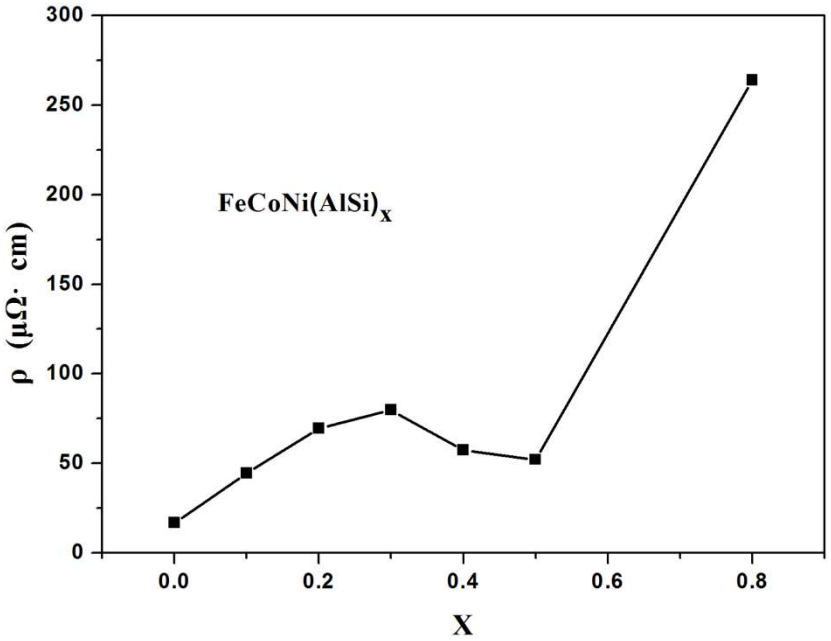


**Figure 2 | The electrical resistivity (ρ) of FeCoNi(AlSi)$_x$ alloys obtained at room temperature.**

been observed in other HEAs[4,27,28]. The FCC-BCC transition with changing composition has been explained from several aspects, such as the valence electron concentration[29] and the lattice distortion and instability[30,31]. Our observation is in general consistent with previous arguments, see the discussion in the supplementary information (Tables S4 and S5, Figures S3 and S4).

To further study the microstructures formed during the rapid solidification, Figure 5 presents the scanning-electron-microstropy (SEM)-backscattered electron images of the alloys. The metallographic pictures taken on a larger length scale can be found in Figure S5. For the A0 alloy, the image in Figure 5(a) indicates a uniform distribution of the elements. Its microstructure is typical of a polycrystalline structure, and the grain size, as measured in Figure S5, varies from 200 μm to 700 μm. Typical cast dendritic and interdendritic structures (labeled by DR and ID, respectively) are observed in A1 to A3 alloys. With more Al and Si contents, the segregation becomes increasingly significant. As the Energy Dispersive X-ray Spectroscopy (EDS) results listed in Table S6 suggest that the ID area is rich in Ni, Si, and Al, while the DR area is rich in Fe and Co. A4 and A5 alloys have similar polycrystalline microstructures, and dendrites can be seen in each grain. The grain size of the A4 alloy (200 μm) is smaller than that in the A5 alloy (300 μm),

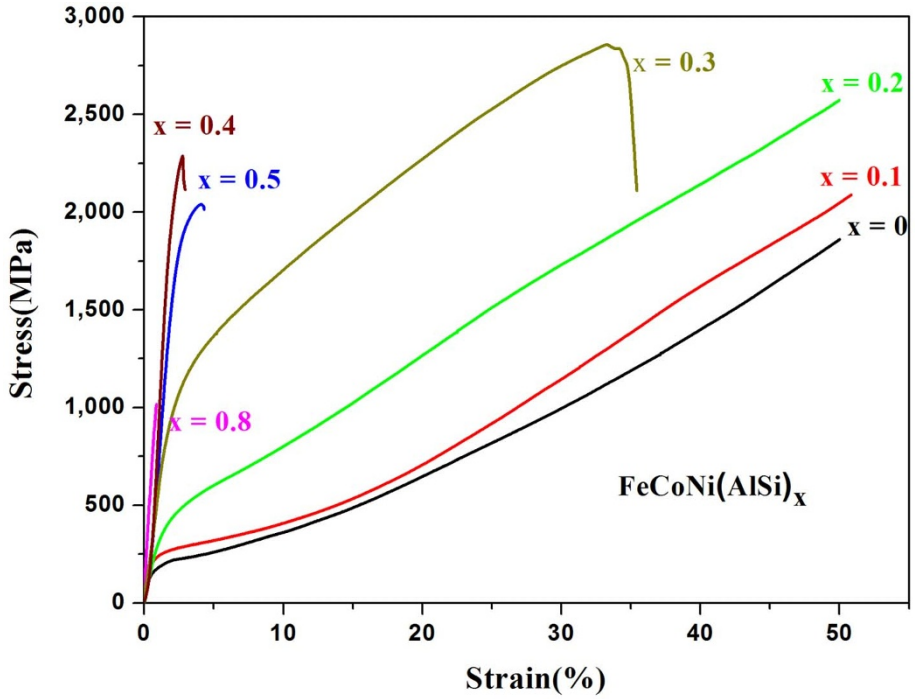


**Figure 3 | Engineering stress-strain curves of FeCoNi(AlSi)$_x$ alloys compressed at a strain rate of 2 × $10^{-4}$/s at room temperature.**

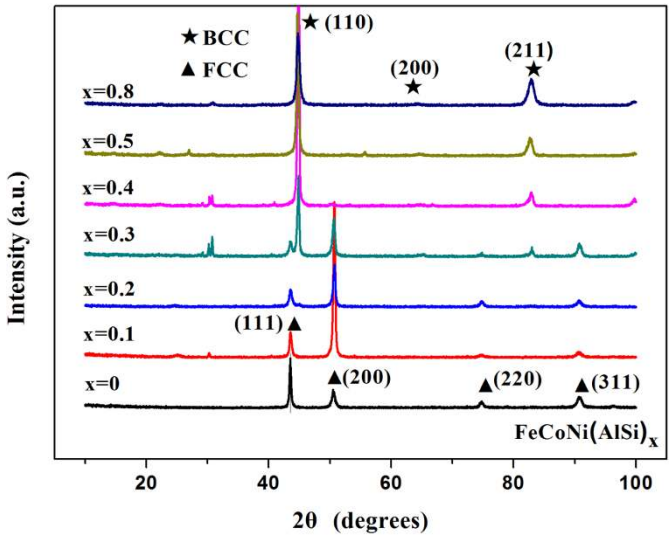


**Figure 4** | XRD patterns of the as-cast $FeCoNi(AlSi)_x$ alloys.

according to Figure S5. The microstructure of the A8 alloy is more complex, as the interdendritic area appears to have three parts [labeled by ID(a), (b), and (c), in the inset of Figure 5(g)]. The white ID(a) area is rich in Ni and Si; the grey ID(b) is rich in Fe and Si; while the flower-like ID(c) is rich in Al and Si. To understand the formation of the above microstructures, it should be first noted that Fe, Co, and Ni are neighbors in the periodic table; their atomic sizes are similar, and their mixing enthalpy is close to zero (Table S5)[32]. When no other species are involved (i.e., A0 alloy), these three elements tend to distribute uniformly, with no obvious segregation detected. The additions of Al and Si break the chemical homogeneity, and the dendritic microsegregation becomes increasingly prominent as x varies from 0 to 0.2. The more Al and Si contents, the more severe the segregation is. There are two possible explanations for this trend. First, Fe and Co have higher melting points than other elements, so that they may solidify first during casting, with the other elements (Ni, Al, and Si) expelled into the ID area. Second, Ni and Si have relatively higher negative mixing enthalpy (Table S5), and they tend to bond with each other. In contrast, the chemical heterogeneity in A4 and A5 alloys is less obvious. This trend seems to suggest that the the BCC phases are more tolerant to chemical randomness,

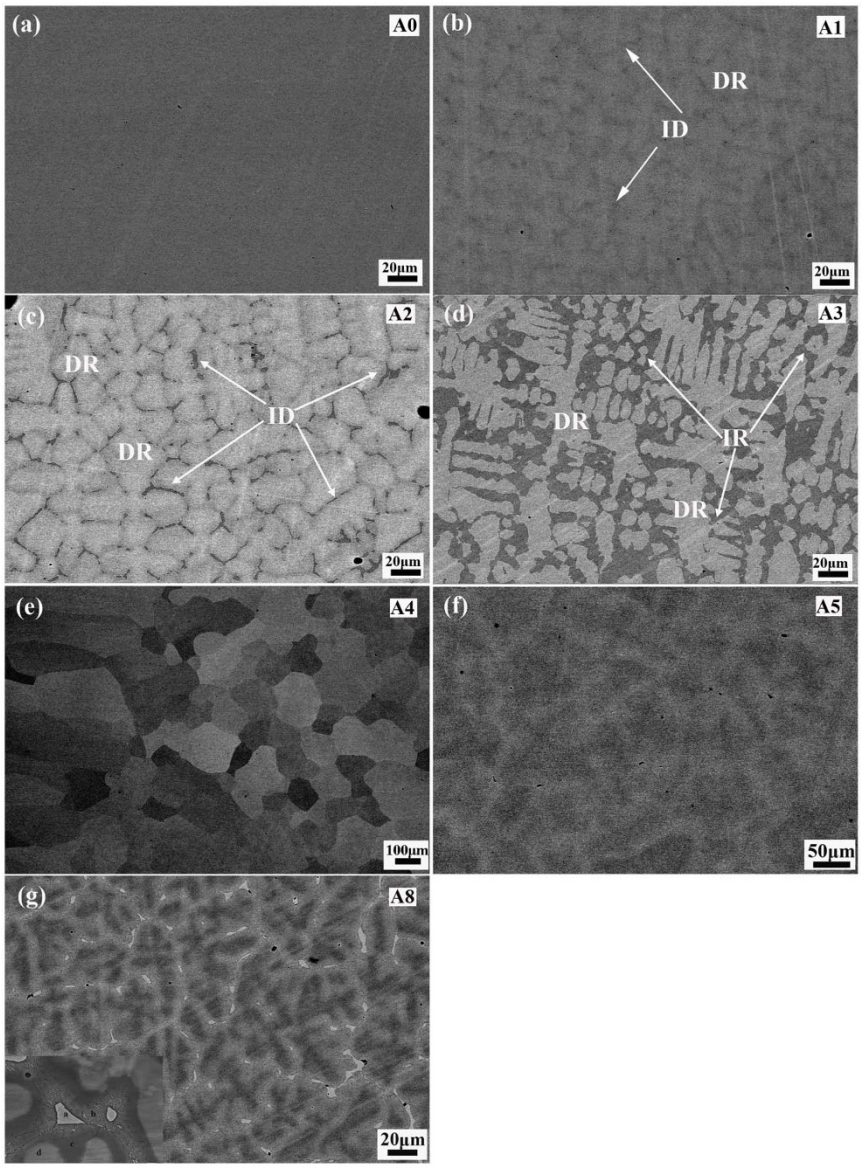


**Figure 5** | SEM backscattering electron images of $FeCoNi(AlSi)_x$ alloys, (a) x = 0, (b) x = 0.1, (c) x = 0.2, (d) x = 0.3, (e) x = 0.4, (f) x = 0.5, and (g) x = 0.8.

compared to the FCC phases in A2 and A3 alloys. In general, the precipitation pathways in multicomponent alloys can be very complex[33], and it is a particularly challenging topic for HEAs, which remains to be studied.

## Discussion

Knowing the structures of the alloys, we are now in a position to discuss the relationship between structures and properties. First of all, the saturation magnetization is primarily determined by the composition and atomic-level structures, and less sensitive to microstructures, such as the grain size and morphology[21]. This trend is demonstrated by its near-monotonic dependence on composition (Figure 1), and allows us to calculate the $M_s$ using the first-principles method. Compared to the previously-studied $Al_xCrFeCoNi$[34], the $M_s$ of our HEAs is much higher (Table S7). The calculated $M_s$ is marked in Figure 1, and the average local magnetic moments are listed in Table S7. It is found that the composition dependence of the $M_s$ in several HEAs is qualitatively reproduced by ab initio calculations, as described in Methods. Quantitatively, the calculated values are systematically higher; this trend is understandable, considering the many possible differences between experiments and simulations. For example, the system size is very limited in simulations, and it also ignores impurities and phase segregation. Nevertheless, our calculations confirm that $FeCoNi(AlSi)_x$ is a much better candidate than $Al_xCrFeCoNi$ for soft-magnetic applications (Table S7), and this trend is mainly because the magnetic moment of Cr is anti-parallel with Fe/Co/Ni (i.e., anti-parallel magnetic coupling), such that magnetization is cancelled out in Cr-containing HEAs (Table S7). The non-magnetic components (Al and Si) are found to be nearly non-polarized (or slightly anti-parallel with Fe/Co/Ni). In addition, HEAs with an FCC structure exhibit much higher saturation magnetization than those with a BCC structure. This feature is due to not only their high contents of the ferromagnetic Fe/Co/Ni, but also the higher atomic packing density (or atomic volume fraction) of the FCC structure. The latter means that for the same composition and elemental magnetic moment, HEAs with an FCC structure should have more (ferromagnetic) atoms (and thus a higher total magnetic moment) per unit volume than those with a BCC structure, yielding higher $M_s$. To summarize, the results of ab initio calculations suggest that to design magnetic HEAs with high $M_s$, one should (1) stay away from Cr, (2) use more Fe and Co and less non-magnetic components, and (3) stabilize the FCC structure.

Different from the saturation magnetization, the coercivity is expected to be sensitive to the grain size, impurity, deformation, and the subsequent heat-treatment process[21]. Specifically, the various microstructures, together with the lattice distortion induced by Al and Si, will inevitably affect the magnetic domain-wall movement and, thus, the coercivity. This effect is the most obvious when x equals 0.3, at which BCC and FCC phases coexist (Figure 4), and the phase boundaries may greatly hinder the domain-wall shift, resulting in the highest coercivity. In alloys of a single-phase structure, such as A4 and A5, the grain size may also matter. For example, the A5 alloy has larger grains than the A4 alloy, such that the domain-wall movement of the A5 alloy is likely to be easier than the A4 alloy, which explains the lower coecivity of the A5 alloy than the A4 alloy. Since $H_c$ is so sensitive to the microstructure, it is likely that at a given composition (and thus $M_s$), the coercivity can be tuned within a fairly-wide range by, for example, the quenching-rate control and heat/pressure treatment. This feature provides opportunities to further reduce the $H_c$ of our alloys.

The additions of Al and Si are expected to elevate the electrical resistivity. As in silicon steels, the Si addition is known to increase the electrical resistivity. Besides, Al has a larger atomic size than other elements, and its addition may lead to larger lattice distortion. The distortion may induce more electron scattering and, thus, reduce the mean free path[25]. This may have contributed to the increased resistivity. Moreover, although HEAs are crystals with long-range order, they may have highly-compromised topological and chemical short-range order[34]. To some extent, HEAs can be considered metals with highly-concentrated point defects, resulting from multiple principal elements in a pseudo-unitary lattice cell, and electronic transportation in these alloys is dominated by the defects[34]. Therefore, the intrinsic structural disorder of HEAs may also contribute to their higher electrical resistivity than that of the corresponding traditional alloys (Table S3). It should be noted that for multi-phase solid solutions, the electrical resistivity is also affected by microstructure, grain size, grain-boundary, and texture[25]. This feature may be responsible for the deviation/fluctuation in the composition range of $0.3 \leq x \leq 0.5$ in Figure 2.

The mechanical properties of HEAs, as in other materials, are closely related to their structures. The increasing strength from the A0 to A2 alloys is believed to stem from the solid-solution-strengthening effect, i.e., the additions of larger Al atoms and smaller Si atoms enhance the crystal lattice distortion, which hinders the movement of the dislocations. For the A3 alloy, which consists of a FCC and BCC structure, its high strength and good plasticity are not only attributed to the increasing lattice distortion[30], but also the fact that the alloy has a mixture of FCC and BCC phases – the FCC structure is known to favor plasticity, and the BCC structure usually has larger lattice resistance for deformation. This trend can be qualitatively justified by considering the friction between sliding planes. The slip along the closest packing planes {110} in the BCC structure is more difficult than that along {111} in the FCC structure, because {110} planes have smaller interplanar spacing and higher lattice friction for dislocation motion[35]. This factor in part also contributes to the diminishing malleability of $FeCoNi(AlSi)_x$ at $x > 4$, when the structure turns almost entirely into a BCC structure. It should be noted that more Si addition also leads to brittleness in the silicon steel.

To summarize, we now have experimentally and theoretically connected the magnetic, electrical, and mechanical properties with the observed atomic-level and micro-scale structures, for the $FeCoNi(AlSi)_x$ HEAs. In particular, we have shown that the alloy with $x = 0.2$ has the best combination of $M_s$ (1.15 T), $H_c$ (1,400 A/m), $\rho$ (69.5 $\mu\Omega\cdot$cm), and $\varepsilon_p$ ($> 50\%$) for applications as SMMs. A comparison with existing SMMs[36–46] in Table S3 further reveals that this high-entropy SMM, in terms of the overall properties, is unique and superb, even though by each particular merit, A2 may not be the best. For example, silicon steels and Fe-Co alloys have higher $M_s$, and nanocrystalline Fe-B-Cu and amorphous Fe-Y-B have higher electrical resistivity. However, the electrical resistivity of Fe-Co alloys is relatively low, and nanocrystalline and amorphous alloys are very brittle. Therefore, when all factors are considered, the A2 alloy stands out and represents a great balance. Moreover, the high corrosion- and wear-resistance of HEAs[14,15] is expected to extend the life time of these high-entropy SMMs under various working conditions. The insight obtained from the present study of composition-dependent structures and properties can be used to guide the design and optimization of structural and functional HEAs, as well as the development of high-entropy SMMs.

## Methods

Ingots with nominal compositions of $FeCoNi(AlSi)_x$ ($x = 0, 0.1, 0.2, 0.3, 0.4, 0.5$, and 0.8, in molar ratios, denoted as A0, A1, A2, A3, A4, A5, and A8, respectively) were prepared by arc-melting pure elements with purity higher than 99.5 weight percent (wt.%) in a high-purity argon atmosphere on a water-cooled Cu hearth. The alloys were remelted four times in order to improve homogeneity. Crystal structures were identified using an X-ray diffractometer under radiation conditions of 30 kV and 20 mA, with a Cu target and a scanning speed of 10°/min. Compressive tests of cylindrical samples with the dimension of $\Phi 3 \times 6$ mm were investigated, using an MTS 809 materials testing machine at room temperature with a strain rate of $2 \times 10^{-4}$ $s^{-1}$. The hardness was measured employing a Vickers hardness tester under a load of 200 g, held for 15 s. The microstructures of cross-sections were examined by a ZEISS SUPRA 55 field emission scanning electron microscope (SEM) with the energy- dispersive spectrometry (EDS) and a ZEISS UMT200i metallographic microscope. The magnetization curves were obtained with the instrument of

"Physical Property Measurement System" (PPMS) made by the "American Quantum Design Company". The electrical resistivity was measured using a Precise Resistance Tester AT510.

Spin-polarized ab initio calculations were performed using the Vienna Ab Initio Simulation Package (VASP)[47], with the Projector Augmented Wave (PAW) method[48]. The Generalized Gradient Approximation (GGA), as implemented by Perdue-Burke-Ernzerhof (PBE)[49], was employed for the exchange-correlation functional. The FCC or BCC lattice was constructed using the experimentally-measured lattice constants, and the cubic supercell (under periodic boundary conditions) contains 108 atoms (FCC) or 128 atoms (BCC). Simulations were conducted at Γ point (the zero point in the reciprocal space) only for structural relaxation, and on a $3 \times 3 \times 3$ Monkhorst-Pack mesh for electronic-structure calculations. To obtain solid solutions, constituent elements in the nominal composition were randomly distributed on the as-constructed lattice. The configurations were then relaxed at 300 K to reproduce the lattice distortion, before the static calculation of the magnetic properties.


1. Yeh, J. W. *et al.* Nanostructured high-entropy alloys with multiple principal elements novel alloy design concepts and outcomes. *Adv. Eng. Mater.* **6**, 299–303 (2004).
2. Senkov, O. N., Wilks, G. B., Scott, J. M. & Miracle, D. B. Mechanical properties of $Nb_{25}Mo_{25}Ta_{25}W_{25}$ and $V_{20}Nb_{20}Mo_{20}Ta_{20}W_{20}$ refractory high entropy alloys. *Intermetallics* **19**, 698–706 (2011).
3. Guo, W. *et al.* Local Atomic structure of a high-entropy alloy: an X-ray and neutron scattering study. *Metall. Mater. Trans. A*, DOI: 10.1007/s11661-012-1474-0 (2012).
4. Tung, C. C. *et al.* On the elemental effect of AlCoCrCuFeNi high-entropy alloy system. *Mater. Lett.* **61**, 1–5 (2007).
5. Tsai, C. W., Chen, Y. L. & Tsai, M. H. Deformation and annealing behaviors of high-entropy alloy $Al_{0.5}CoCrCuFeNi$. *J. Alloys Compd.* **486**, 427–435 (2009).
6. Shun, T. T. & Du, Y. C. Microstructure and tensile behaviors of FCC $Al_{0.3}CoCrFeNi$ high entropy alloy. *J. Alloys Compd.* **479**, 157–160 (2009).
7. Hemphill, M. A. *et al.* Fatigue behavior of $Al_{0.5}CoCrCuFeNi$ high-entropy alloys. *Acta Mater.* **60**, 5723–5734 (2012).
8. Lin, C. M. & Tsai, H. L. Evolution of microstructure, hardness, and corrosion properties of high-entropy $Al_{0.5}CoCrFeNi$ alloy. *Intermetallics* **19**, 288–294 (2011).
9. Wang, Y. P., Li, B. S. & Fu, H. Z. Solid solution or intermetallics in a high-entropy alloy. *Adv. Eng. Mater.* **11**, 641–644 (2009).
10. Singh, S., Wanderka, N., Murty, B. S., Glatzel, U. & Ban, J. Decomposition in multi-component AlCoCrCuFeNi high-entropy alloy. *Acta Mater.* **59**, 182–190 (2011).
11. Zhang, K. B. Nanocrystalline CoCrFeNiCuAl high-entropy solid solution synthesized by mechanical alloying. *J. Alloys Compd.* **485**, L31–L34 (2009).
12. Tsai, M. H., Yeh, J. W. & Gan, J. Y. Diffusion barrier properties of AlMoNbSiTaTiVZr high-entropy alloy layer between copper and silicon. *Thin Solid Films* **516**, 5527–5530 (2008).
13. Senkov, O. N., Wilks, G. B., Miracle, D. B., Chuang, C. P. & Liaw, P. K. Refractory high-entropy alloys. *Intermetallics* **18**, 1758–1765 (2010).
14. Huang, C., Zhang, Y. Z., Shen, J. Y. & Vilar, R. Thermal stability and oxidation resistance of laser clad TiVCrAlSi high entropy alloy coatings on Ti–6Al–4V alloy. *Surf. Coat. Technol.* **206**, 1389–1395 (2011).
15. Chuang, M. H., Tsai, M. H., Wang, W. R., Lin, S. J. & Yeh, J. W. Microstructure and wear behavior of $Al_xCo_{1.5}CrFeNi_{1.5}Ti_y$ high-entropy alloys. *Acta Mater.* **59**, 6308–6317 (2011).
16. Senkov, O. N., Scott, J. M., Senkova, S. V., Miraclea, D. B. & Woodwarda, C. F. Microstructure and room temperature properties of a high-entropy TaNbHfZrTi alloy. *J. Alloys Compd.* **509**, 6043–6048 (2011).
17. Kuznetsov, A. V., Shaysultanov, D. G., Stepanov, N. D., Salishchev, G. A. & Senkov, O. N. Tensile properties of an AlCrCuNiFeCo high-entropy alloy in as-cast and wrought conditions. *Mater. Sci. Technol. A* **533**, 107–118 (2012).
18. Lucas, M. S. & Mauger, L. Magnetic and vibrational properties of high-entropy alloys. *J. Appl. Phys.* **109**, 07E307 (2011).
19. Osaka, T. *et al.* A soft magnetic CoNiFe film with high saturation magnetic flux density and lowcoercivity. *Nature* **392**, 796–798 (1998).
20. Fu, H. D., Zhang, Z. H., Yang, Q. & Xie, J. X. Morphology of the boron-rich phase along columnar grain boundary and its effect on the compression crack of Fe–6.5Si–0.05B alloy. *Mater. Sci. Eng., A* **528**, 1425–1430 (2011).
21. Sun, G. F. & Qiang, W. J. *Magnetic material* (Chemical Industry Press, Beijing, 2007).
22. Hasegawa, R. Present status of amorphous soft magnetic alloys. *J. Magn. Magn. Mater.* **215–216**, 240–245 (2000).
23. Hasegawa, R. Applications of amorphous magnetic alloys. *Mater. Sci. Eng. A* **375–377**, 90–97 (2004).
24. Greer, L. A. Metallic glasses. *Science, New Series* **267**, 1947–1953 (1995).
25. Qiu, C. J., Wang, Y. H. & Qu, W. *Material Physical Properties* (Harbin Industry Technology Univ. Press, Harbin, 2009).
26. Sun, G. F. & Qiang, W. J. *Magnetic material* (Chemical Industry Press, Beijing, 2007).
27. Chou, H. P., Chang, Y. S., Chen, S. K. & Yeh, J. W. Microstructure, thermophysical and electrical properties in $Al_xCoCrFeNi$ ($0 \le x \le 2$) high-entropy alloys. *Mater. Sci. Eng. B* **163**, 184–189 (2009).
28. Li, C., Li, J. C., Zhao, M. & Jiang, Q. Effect of alloying elements on microstructure and properties of multiprincipal elements high-entropy alloys. *J. Alloys Compd.* **475**, 752–757 (2009).
29. Guo, S., Ng, C., Lu, J. & Liu, C. T. Effect of valence electron concentration on stability of fcc or bcc phase in high entropy alloys. *J. Appl. Phys.* **109**, 103505 (2011).
30. Wang, F. J., Zhang, Y. & Chen, G. L. Atomic packing efficiency and phase transition in a high entropy alloy. *J. Alloys Compd.* **478**, 321–324 (2009).
31. Zhang, Y., Zhou, Y. J., Lin, J. P., Chen, G. L. & Liaw, P. K. Solid solution phase formation rules for multi-component alloys. *Adv. Eng. Mater.* **10**, 534–538 (2008).
32. Takeuchi, A. & Inoue, A. Classification of bulk metallic glasses by atomic size difference, heat of mixing and period of constituent elements and its application to characterization of the main alloying element. *Mater. Trans.* **12**, 2817–2829 (2005).
33. Clouet, E. *et al.* Complex precipitation pathways in multicomponent alloys. *Nat. Mater.* **5**, 482–488 (2006).
34. Kao, Y. F., Chen, S. K. & Chen, T. J. Electrical, magnetic, and Hall properties of $Al_xCoCrFeNi$ high-entropy alloys. *J. Alloys Compd.* **509**, 1607–1614 (2011).
35. Hu, G. X., Cai, X. & Rong, Y. H. *Fundamentals of Materials Science* (Shanghai Jiao Tong Univ. Press, Shanghai, 2006).
36. Alves, F., Lebourgeois, R. & Waeckerle, T. Soft magnetic materials for electrical engineering: State of the art and recent advances. *Euro. Trans. Electr. Power.* **15**, 467–479 (2005).
37. Lv, Q. C. *et al.* Note on magnetic properties of grain oriented 4%Si-Fe. *Acta Metall Sin.* **20**, B127–B130 (1984).
38. Liang, Y. F. Fabrication and properties of Fe-6.5%Si alloy sheet by cold rolling. Doctoral Dissertation, University of Science and Technology Beijing (2010).
39. Tang, J. C., Hu, D. P., Tai, Z. Z., Huang, B. Y. & Liu, W. S. Microstructures and soft magnetic properties of nanocrystalline $Fe_{86}B_{13}Cu_1$ alloy annealed by hot isothermal pressing. *J. Alloys Compd.* **493**, 134–136 (2010).
40. Inoue, A., Shen, B. L., Koshiba, H., Kato, H. & Yavari, A. R. Ultra-high strength above 5000 MPa and soft magnetic properties of Co–Fe–Ta–B bulk glassy alloys. *Acta Mater.* **52**, 1631–1637 (2004).
41. Huang, Y. J., Li, S. K. & Lan, Z. W. *Magnetic Materials* (Electronic Industry Press, Beijing, 1994).
42. Lin, C. Y., Lee, M. C. & Chin, T. S. Fe–Y–M–B (M = Nb or Ta) bulk metallic glasses with ultrahigh strength and good soft magnetic properties. *J. Phys. D: Appl. Phys.* **40**, 310–314 (2007).
43. Davis, J. R. *ASM Specialty Handbook: Nickel, Cobalt, and Their Alloys* (ASM International Handbook Committee, Ohio, USA. 2000).
44. Ren, L., Basu, S., Hai, Y. R., Xiao, J. Q. & Parvizi-Majidi, A. Mechanical properties of Fe-Co soft magnets. *J. Mater. Sci.* **36**, 1451–1457 (2001).
45. Hu, Q. X., Sun, G. F., Chen, J. F., Chen, Q. A. & Chen, Y. Study on magnetic properties and mechanical properties of Fe-Co soft magnetic materials. *Metallic Functional Material.* **12**, 24–27 (2005).
46. Inoue, A., Shen, B., Koshiba, H., Kato, H. & Yavari, A. R. Cobalt-based bulk glassy alloy with ultrahigh strength and soft magnetic properties. *Nat. Mater.* **2**, 661–663 (2003).
47. Kresse, G. & Furthmüller, J. Efficient iterative schemes for ab initio total-energy calculations using a plane-wave basis set. *Phys. Rev. B* **54**, 11169–11186 (1996).
48. Blochl, P. E. Projector augmented-wave method. *Phys. Rev. B* **50**, 17953–17979 (1994).
49. Perdew, J. P., Burke, K. & Ernzerhof, M. Generalized gradient approximation made simple. *Phys. Rev. Lett.* **77**, 3865–3868 (1996).


## Acknowledgments

The authors would like to acknowledge the financial support by the Natural Science Foundation of China (NSFC, No.50971019). PKL appreciates the support from the US National Science Foundation (DMR-0909037, CMMI-0900271, and CMMI-1100080), the Department of Energy (DOE) Office of Nuclear Energy's Nuclear Energy University Program (NEUP) 00119262, and the DOE, Office of Fossil Energy, National Energy Technology Laboratory (DE-FE-0008855) with Drs. C.V. Cooper, A. Ardell, E.M. Taleff, R.O. Jensen, Jr., Lizhen Tan, V. Cedro, and S. Lesica as program managers. YQC is supported by the Scientific User Facilities Division, Office of Basic Energy Sciences, US Department of Energy. This work used computational resources provided by the Center for Nanophase Materials Sciences, Oak Ridge National Laboratory, and the Extreme Science and Engineering Discovery Environment (XSEDE), which is supported by National Science Foundation grant number OCI-1053575.

## Author contributions

All authors have made contributions to this paper. Y. Zhang and T.T. Zuo conducted the experiments and wrote the paper; Y.Q. Cheng performed the theoretical calculation and wrote the paper; Y. Zhang and P.K. Liaw designed the experiments and revised the paper. All authors discussed the results and reviewed the manuscript.

## Additional information

**Supplementary information** accompanies this paper at http://www.nature.com/scientificreports

**Competing financial interests:** The authors declare no competing financial interests.



**How to cite this article:** Zhang, Y., Zuo, T., Cheng, Y. & Liaw, P.K. High-entropy Alloys with High Saturation Magnetization, Electrical Resistivity, and Malleability. *Sci. Rep.* **3**, 1455; DOI:10.1038/srep01455 (2013).